Cellular and Molecular Life Sciences (2024) 81:37
https://doi.org/10.1007/s00018-023-05029-7

ORIGINAL ARTICLE

Early endocannabinoid-mediated depolarization-induced suppression of excitation delays the appearance of the epileptic phenotype in synapsin II knockout mice

Nicola Forte[1] · Alessandro Nicois[1] · Brenda Marfella[1] · Isabella Mavaro[1] · Livia D'Angelo[2] · Fabiana Piscitelli[1] · Anna Scandurra[3] · Paolo De Girolamo[2] · Pietro Baldelli[4,6] · Fabio Benfenati[5,6] · Vincenzo Di Marzo[1,7,8,9] · Luigia Cristino[1]

Received: 13 June 2023 / Revised: 16 October 2023 / Accepted: 31 October 2023

Abstract

The mechanism underlying the transition from the pre-symptomatic to the symptomatic state is a crucial aspect of epileptogenesis. *SYN2* is a member of a multigene family of synaptic vesicle phosphoproteins playing a fundamental role in controlling neurotransmitter release. Human *SYN2* gene mutations are associated with epilepsy and autism spectrum disorder. Mice knocked out for synapsin II (SynII KO) are prone to epileptic seizures that appear after 2 months of age. However, the involvement of the endocannabinoid system, known to regulate seizure development and propagation, in the modulation of the excitatory/inhibitory balance in the epileptic hippocampal network of SynII KO mice has not been explored. In this study, we investigated the impact of endocannabinoids on glutamatergic and GABAergic synapses at hippocampal dentate gyrus granule cells in young pre-symptomatic (1–2 months old) and adult symptomatic (5–8 months old) SynII KO mice. We observed an increase in endocannabinoid-mediated depolarization-induced suppression of excitation in young SynII KO mice, compared to age-matched wild-type controls. In contrast, the endocannabinoid-mediated depolarization-induced suppression of inhibition remained unchanged in SynII KO mice at both ages. This selective alteration of excitatory synaptic transmission was accompanied by changes in hippocampal endocannabinoid levels and cannabinoid receptor type 1 distribution among glutamatergic and GABAergic synaptic terminals contacting the granule cells of the dentate gyrus. Finally, inhibition of type-1 cannabinoid receptors in young pre-symptomatic SynII KO mice induced seizures during a tail suspension test. Our results suggest that endocannabinoids contribute to maintaining network stability in a genetic mouse model of human epilepsy.

Keywords Endocannabinoids · CB1 · Dentate gyrus · Epileptogenesis

✉ Vincenzo Di Marzo
vincenzo.dimarzo@criucpq.ulaval.ca

✉ Luigia Cristino
luigia.cristino@icb.cnr.it

1 Institute of Biomolecular Chemistry, National Research Council of Italy, Pozzuoli (NA), Italy

2 Department of Veterinary Medicine and Animal Production, University of Naples Federico II, Naples, Italy

3 Department of Biology, University of Naples Federico II, Naples, Italy

4 Department of Experimental Medicine, University of Genoa, Genoa, Italy

5 Center for Synaptic Neuroscience and Technology, Istituto Italiano di Tecnologia, Genoa, Italy

6 IRCCS Ospedale Policlinico San Martino, Genoa, Italy

7 Faculty of Medicine and Faculty of Agricultural and Food Sciences, Canada Excellence Research Chair on the Microbiome-Endocannabinoidome Axis in Metabolic Health, Université Laval, Québec City, QC, Canada

8 Heart and Lung Research Institute of Université Laval, Québec City, QC, Canada

9 Institute for Nutrition and Functional Foods, Centre NUTRISS, Université Laval, Québec City, QC, Canada

Published online: 12 January 2024

Introduction

It is estimated that approximately 50 million people worldwide suffer from epilepsy, making it one of the most common neurological disorders [1]. The development of novel therapeutical approaches is crucial since more than 30% of patients experience epileptic seizures despite the treatments [2]. The mechanisms promoting the transition from the pre-epileptic to the epileptic state remain largely unclear. Temporal lobe epilepsy (TLE) is the most common type of epilepsy [3] and intractable TLE is often successfully mitigated only by excision of the hippocampus and adjacent regions of the brain [4]. This brain area indeed is highly prone to develop seizures and provides a model to study epileptiform events and epileptogenesis both ex vivo and in vitro.

The dentate gyrus (DG) of hippocampus plays a primary role in TLE [5, 6]. This area is anatomically and functionally defined by its tightly clustered, hyperpolarized granule cells (GCs), which are controlled locally by excitatory hilar mossy cells (MCs) and by various types of inhibitory interneurons [7, 8]. GCs filter and integrate the synaptic inputs that receive from the perforant pathway and thus represent a gate to the spread of the excitatory signals originating from the entorhinal cortex [5, 8]. While the most common type of central nervous system synapse is the "*non-detonator*" synapse, characterized by a relatively low success rate in triggering spikes in postsynaptic targets [9], GC to CA3 mossy-fiber synapses in the hippocampus have been referred to as "*detonator*" synapses as, in the presence of a burst of presynaptic activity, they can strongly activate the CA3 postsynaptic pyramidal cells to form an epileptic focus [6, 10, 11]. These features make the DG-GC neurons an interesting substrate to study the functional alterations of this neuro-anatomical pathway in epilepsy.

Synapsin II (*SYN2*), a member of the multigene synapsin family of synaptic vesicle phosphoproteins (*SYN1/2/3*), plays a major role in the control of neurotransmitter release in the hippocampus [12–17] SynII KO mice are prone to develop epilepsy [18] and an intronic polymorphism in the *SYN2* gene is associated to idiopathic epilepsy [19, 20]. Mutant mice lacking *SYN2* are all prone to develop spontaneous epileptic seizures after 2–3 months of age [21], although it was reported that occasional seizures can be elicited in younger mice under stressful conditions (tail suspension test, TST) [17]. SynI and SynII mutant mice, but not SynIII mutants are epileptic, with SynII KO mice showing the more severe epileptic phenotype [21]. The transition phase before the full establishment of an epileptic phenotype offers interesting possibilities to study the mechanisms which underlie epileptogenesis [12]. Several alterations, potentially leading to epilepsy, have been reported in the hippocampal DG network of SynII KO, such as: (1) an increased excitation/inhibition (E/I) ratio in the MCs to the GCs microcircuit [12], (2) a decreased asynchronous GABA release [13] and subsequent reduction of GABAergic tonic inhibition [14], and (3) an alteration of adult hippocampal neurogenesis and BDNF levels [22, 23].

The endocannabinoids (eCBs), 2-arachidonoylglycerol (2-AG) and anandamide (AEA), by acting at type-1 cannabinoid receptors (CB1R), contribute to the maintenance of the local balance of the E/I ratio [24, 25] and are altered in TLE [26]. The eCBs are neuromodulators synthesized "on demand" by postsynaptic neurons in response to neuronal depolarization; the subsequent retrograde activation of CB1Rs expressed on presynaptic terminals in turn inhibits synaptic transmission by reducing neurotransmitter release [25, 27]. The activation of CB1Rs in glutamatergic terminals leads to a phenomenon known as depolarization-induced suppression of excitation (DSE), whereas activation of CB1Rs in GABAergic terminals leads to depolarization-induced suppression of inhibition (DSI) [27, 28]. Depending on the distribution of CB1Rs between glutamatergic and GABAergic inputs, eCBs can decrease or exacerbate epileptic seizures, respectively, by affecting the hippocampal E/I balance, a condition of critical relevance for shaping the functional connectivity of the hippocampus in epileptogenesis [24].

With the present study, we sought to determine whether changes in eCB signalling might contribute to the switch from the pre-symptomatic to the symptomatic phase of the SynII KO phenotype. With this purpose, we performed electrophysiological, immunohistochemical, behavioural, and biochemical studies of eCB signalling at CB1Rs in the DG of young pre-symptomatic and adult epileptic SynII KO mice.

Materials and methods

Animals

The study was performed according to the ARRIVE Guidelines to improve the reporting of bioscience research using laboratory animals. Experiments were performed following the European Union animal welfare guidelines [European Communities Council Directive of September 22, 2010 (2010/63/EU)] and the Italian Decree (n.26/2014, authorization n. 783/2020)**.** Experiments were performed on 1- to 2-month-old and 5- to 8-month-old adult Syn II KO male mice generated by homologous recombination and on age-matched C57BL/6 J wild-type (WT) animals.

Slice preparation and electrophysiological recordings

Mice were anaesthetized with an overdose of isoflurane, quickly decapitated and the brain was cut in horizontal slices of 400 µm using a Leica VT1000 S Vibrating blade microtome at 3–5 °C in a solution containing (in mM): 87 NaCl, 25 $NaHCO_3$, 2.5 KCl, 0.5 $CaCl_2$, 7 $MgCl_2$, 25 glucose, 75 sucrose, and saturated with 95% O_2 and 5% CO_2. The artificial cerebrospinal fluid used for recordings contained (in mM): 125 NaCl, 25 $NaHCO_3$, 25 glucose, 2.5 KCl, 1.25 NaH_2PO_4, 2 $CaCl_2$, and 1 $MgCl_2$, pH 7.3 gassed with 95% O_2–5% CO_2. Slices were left to recover for 1 h at 35 °C and 30 min at RT in recording solution. Whole-cell recordings (holding potential = − 80 mV) were performed at RT with a Multiclamp 700B/Digidata1440A system (Molecular Devices, Sunnyvale, CA) on visually identified mature GCs using a Leica DM6000 FS microscope equipped with a WAT-902H Ultimate camera. We selected GCs for recording based on their oval shape and central location in the granule layer. As GCs can exist in various stages of maturation, we only recorded from mature neurons with a resting membrane resistance of less than 300 MΩ [29].

The excitatory synaptic activity was recorded using a K-gluconate-based intracellular solution containing (in mM): 126 K gluconate, 4 NaCl, 1 $MgSO_4$, 0.02 $CaCl_2$, 0.1 BAPTA, 15 glucose, 5 HEPES, 3 MgATP, and 0.1 NaGTP, pH 7.3, 290 mosm/l. Evoked excitatory postsynaptic currents (eEPSCs) and spontaneous excitatory postsynaptic currents (sEPSCs) were recorded in the presence of bicuculline (30 µM), CGP 55845 (5 µM) (Tocris Bioscience, Ellisville, MO) to inhibit $GABA_A$ and $GABA_B$ receptors, respectively. The inhibitory synaptic activity was recorded using a high chloride intracellular solution containing (in mM): 126 KCl, 4 NaCl, 1 $MgSO_4$, 0.02 $CaCl_2$, 0.1 BAPTA, 15 glucose, 5 HEPES, 3 ATP, and 0.1 GTP, pH 7.3 with KOH, 290 mosm/L. Evoked inhibitory postsynaptic currents (eIPSCs) and spontaneous inhibitory postsynaptic currents (sIPSCs) were recorded in the presence of D-APV (50 µM), CNQX (10 µM) (Tocris Bioscience, Ellisville, MO) to inhibit NMDA and AMPA receptors. AM251 (4 µM) and ACEA (125 nM) (Tocris) were used in a subset of experiments to inhibit or activate CB1R respectively. The patch pipette resistance was 4–7 MΩ when filled with intracellular solution. eEPSCs and eIPSCs were recorded in response to extracellular stimulation with a monopolar glass electrode connected with an isolated pulse stimulator AM 2100 (A-M Systems, Carlsborg, WA) and placed in the proximity of the recorded GC in the molecular layer field. The stimulation intensity to obtain a minimal response was identified (50–80 µA for 50 µs), as previously demonstrated [13], while the input/output curves were performed with increasing stimulation intensities from 10 to 250 µM for 50 µs. All data were acquired with Clampex and analysed offline with Clampfit 11.2 (Molecular Devices, Sunnyvale CA, USA), Excel, and GraphPad.

Lipid extraction and endocannabinoids measurement

Tissue samples were pooled and analysed using liquid chromatography–atmospheric pressure chemical ionization–mass spectrometry (LC–APCI–MS; LabSolution Shimadzu). The eCB 2-AG was extracted from tissues and then purified and quantified as previously described. First, hippocampal tissues were pooled and homogenized in 5 vol chloroform/methanol/ Tris–Cl 50 mM pH 7.5 (2:1:1 by volume) containing 10 pmol of d^8—AEA and 50 pmol of d^5-2-AG as internal deuterate standard. Homogenates were centrifuged at 13,000 × g for 16 min (4 °C), and the aqueous phase plus debris were collected and four times extracted with 1 vol chloroform. The lipid-containing organic phases were dried and pre-purified by open-bed chromatography on silica columns eluted with increasing concentrations of methanol in chloroform. Fractions for AEA and 2-AG measurement were obtained by eluting the columns with 9:1 (by volume) chloroform/methanol and then analszed by LC–APCI–MS. LC–APCI–MS analyses were carried out in the selected ion monitoring mode, using m/z values of 356 and 348 (molecular ions + 1 for deuterated and non-deuterated AEA), 384.35 and 379.35 (molecular ions + 1 for deuterated and non-deuterated 2-AG). AEA and 2-AG levels were, therefore, calculated based on their area ratios with the internal deuterated standard signal areas. Values are expressed as pmol/mg of wet tissue extracted.

Immunohistochemistry

Three animals/group were deeply anesthetized and transcardially perfused with physiological saline and subsequently with 4% paraformaldehyde, pH 7.4. Brains were cut with a Leica CM3050S cryostat into 10-µm thick serial coronal sections, collected in alternate series and processed for immunofluorescence. Anatomic comparable sections of the hippocampus were processed for multiple immunoreactivities after incubation for 1 h at RT in phosphate buffer (PB) containing 0.3% Triton and 5% donkey serum (blocking buffer). Sections were then incubated overnight at 4 °C with the mix of primary antibodies diluted in donkey serum. The following primary antibodies were used: guinea pig anti-VGluT1 (1:200; SYSY, cat. no. 135 304); rabbit anti-CB1 receptor antibody (anti-C-terminus 461–472, Abcam, ab23703, 1:300), guinea pig anti-VGAT (1:200, SYSY, cat. no. 131 004), goat anti-CB1 receptor antibody (anti-C-terminus 461–472, Abcam; ab40860; 1:300), rabbit anti-DGAL antibody (1:500) and goat anti-MAGL antibody

(1:200; Abcam, cat. no. ab77398). After incubation with primary antibodies, sections were washed with PB and immunofluorescence revealed by specific Alexa secondary donkey anti-IgGs (Invitrogen, ThermoFisher Scientific, France): Alexa-350 donkey anti-goat (A21081, 1:150); Alexa-350 donkey anti-rabbit (A10039, 1:100 or 1:150); Alexa-488 donkey anti-rabbit (A21206, 1:150); Alexa-488 goat anti-guinea pig (A11073, 1:100); Alexa-594 donkey anti-goat (A11058, 1:50). Sections were counterstained with DAPI (Sigma–Aldrich) to detect nuclei, mounted with Prolong Gold (Invitrogen), and coverslipped with Aquatex mounting medium (Merck, Darmstadt, Germany). The immunostained sections were observed with a Nikon Eclipse Ti2 confocal microscope (Nikon, Florence, Italy) equipped with an x–y–z motorized stage, a digital camera DS-Qi2 and the acquisition and image analysis software NIS-Elements C (Nikon, The Netherlands). Digital serial Z-stacks images were collected throughout the area of interest ($n \leq 20$ planes with an increment of 0.5 µm).

Image analysis

For the quantification of single or double immunolabeling, serial Z plane images were collapsed into two-dimensional images ($n \leq 20$ planes with an increment 0.5 µm). To measure the percentages of CB1 colocalization in VGAT- and VGLUT1-immunoreactive areas of DG, an unbiased physical dissector-based counting of CB1/VGAT or CB1/VGLUT1 double immunoreactive puncta was performed following the protocols described in Bolte and Cordelières [30]. Puncta were counted throughout the anterior – posterior axis of the GC layer in a series of 10 µm VGAT- or VGLUT1-immunolabeled coronal sections spaced 160 µm apart (1:8 as the frequency of section sampling for the cell count) starting from Bregma – 1.40 mm up to Bregma – 3.00 mm, to cover the complete rostro-caudal extension of the DG. All analysis were conducted by an observer blinded to the experimental design using an image processing package of ImageJ software developed by the National Institutes of Health.

Behavioural analysis

Behavioural experiments were performed during the standard light phase between 2:00 and 5:00 pm. One-month-old mice (WT and SynII KO) were suspended by the tail for 3 min and video-recorded. This protocol was reported to elicit occasional seizures in P15-P30 SynII KO mice [17]. Videos were later transferred to a personal computer for digital storage and visually analysed using Solomon Coder® beta 16.06.26 (ELTE TTK, Hungary). Data were blind coded by an experienced researcher, while a second independent researcher randomly coded approximately 20% of the total videos to test inter-observer reliability. The level of agreement ranged from 93 to 99%. The behaviour observed in 3 min videos were recorded and categorized into three classes: Immobility, Movement, and Seizure. When the animals exhibit small movements confined to the forelimbs, without the involvement of the hindlimbs or pendulum-like swings due to momentum gained during earlier mobility phases [31], were recorded as Immobility. The escape-oriented body movements (bend the torso sideways to touch the tail or back of the body) and any movement not attributable to an epileptic seizure were included in the Movement category. Seizure events were characterized by *opisthotonus* events (acute or chronic spastic arching of the neck and back), forelimb and hindlimb myoclonus. All behaviours

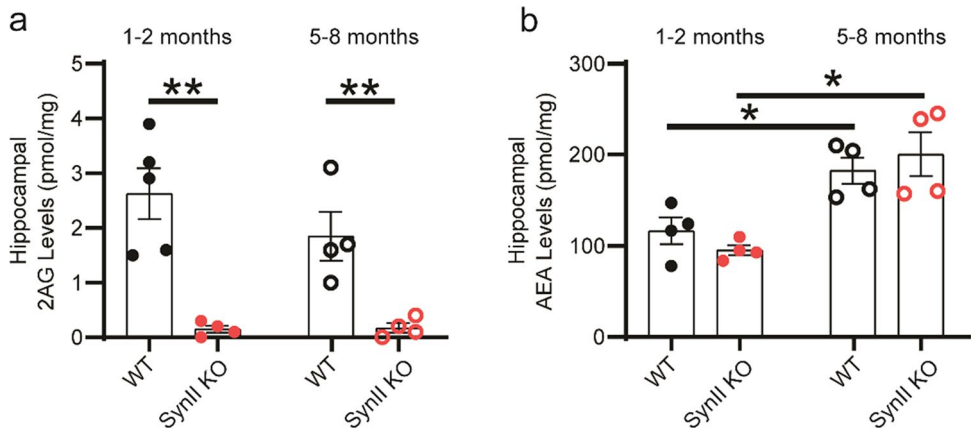

Fig. 1 Hippocampal endocannabinoid 2-AG levels are decreased in SynII KO mice. **a** Bar graph of hippocampal 2-AG levels (pmol/mg) in 1/2-month-old and 5/8-month-old WT (2.60 ± 0.4 and 1.85 ± 0.40 pmol/mg, respectively) and SynII KO mice (0.15 ± 0.06 and 0.17 ± 0.08 pmol/mg, respectively). $^{**}p < 0.01$, two-way ANOVA ($F_{1.13} = 34.29$)/Tukey's tests. **b** Bar graph of hippocampal AEA levels (pmol/mg) in 1/2-month-old and 5/8-month-old WT (116.5 ± 14.34 and 182.30 ± 14.46 pmol/mg, respectively) and SynII KO mice (95.50 ± 5.30 and 200.30 ± 24.14 pmol/mg, respectively). $^{*}p < 0.05$, two-way ANOVA ($F_{1.12} = 28.31$)/Tukey's tests

were recorded in duration (i.e., the amount of time expressed in %) and latency (i.e., the time elapsed from the start of the test until the first observation of the behaviour). Three days after the recording session with vehicle, the AM251 (3 mg/kg) or JZL184 (8 mg/kg, once per day for three days) was administered intraperitoneally and the test was repeated 30 min after the last injection.

Statistics

All data are expressed as means ± s.e.m. All statistics were performed with GraphPadPrism® (GraphPad Software Inc., San Diego, CA, USA). The Shapiro–Wilk test was first applied to confirm the normal distribution of the data. For comparison between WT and SynII KO experiments, a

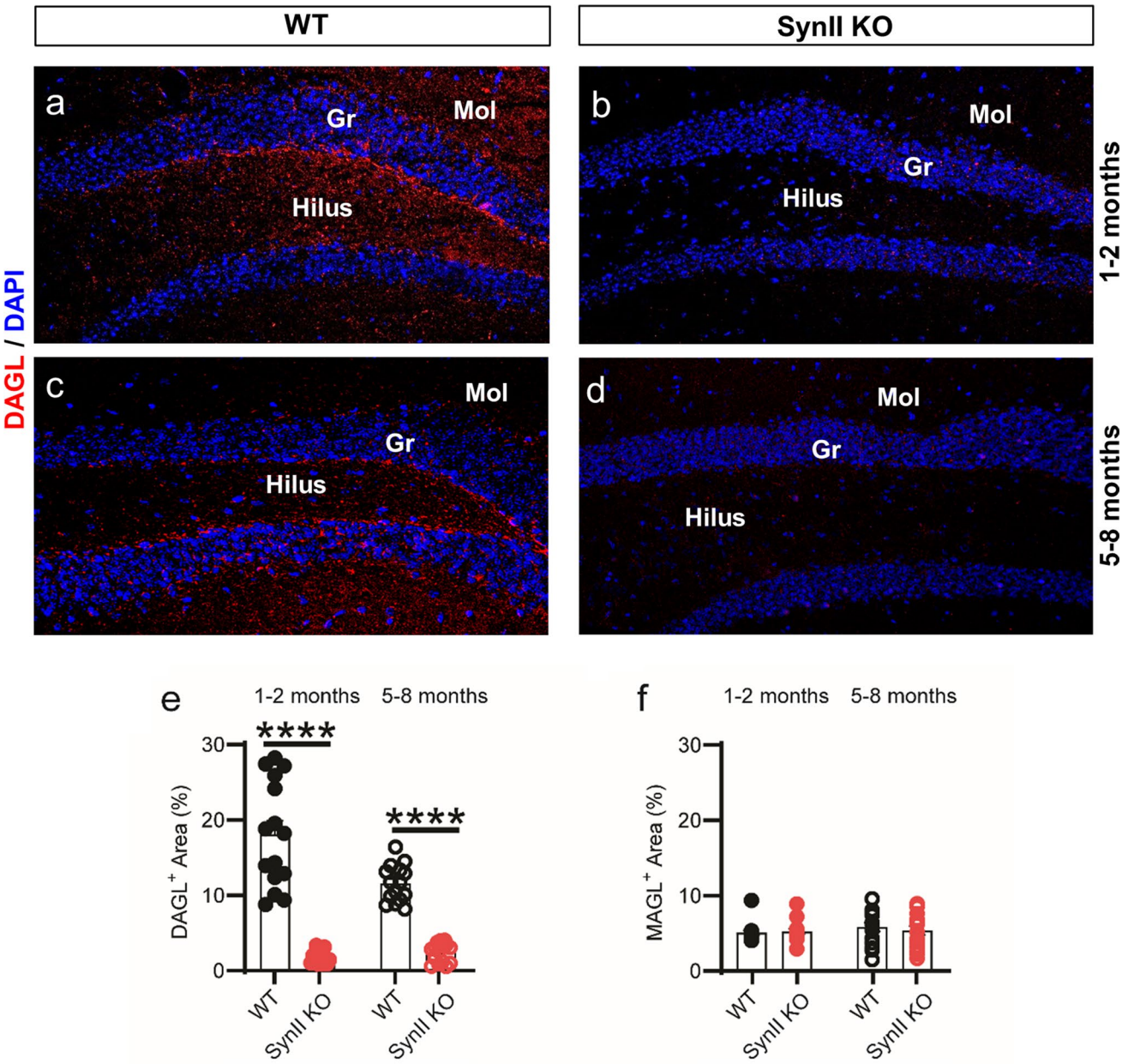

Fig. 2 Distribution of DAGL immunoreactivity in the dentate gyrus of young and adult SynII KO mice. **a–d** DAGL/DAPI immunolabeling of the DG showing the reduction of DAGL expression in SynII KO in comparison to age-matched WT mice. **e** Bar graph showing the percentage of DAGL immunoreactivity areas in 1/2-month-old and 5/8-month-old mice. $n = 15$ sections per group in three mice; $WT_{1/2} = 18.1 \pm 1.8\%$, SynII $KO_{1/2} = 1.9 \pm 0.2\%$, $WT_{5/8} = 11.57 \pm 0.6\%$, SynII $KO_{5/8} = 2.4 \pm 0.3\%$. $^{****}p < 0.0001$, two-way ANOVA ($F_{1.56} = 167.1$) /Tukey's tests. **f** Bar graph showing the percentage of MAGL immunoreactivity areas in 1/2-month-old and 5/8-month-old mice. $n = 15$ sections per group in three mice; $WT_{1/2} = 4.7 \pm 0.1\%$, SynII $KO_{1/2} = 5.25 \pm 0.3\%$, $WT_{5/8} = 7.8 \pm 0.4\%$, SynII $KO_{5/8} = 5.53 \pm 0.59\%$

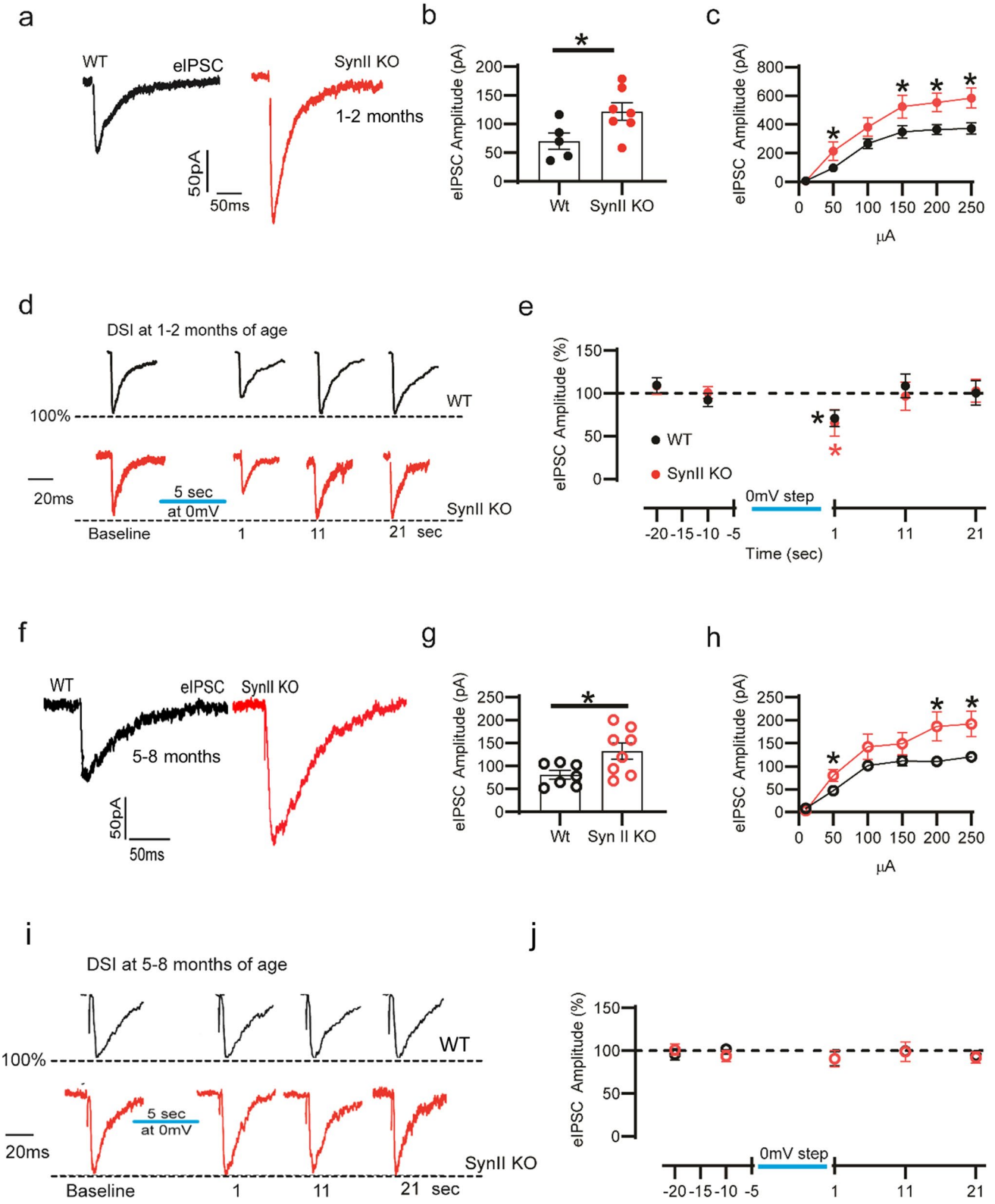

two-tailed unpaired Student's *t* test or Wilcoxon matched-pairs signed rank test was used. For intergroup comparison in DSI and DSE experiments, the one-sample Student's *t* test was used. For multiple comparisons, two-way ANOVA with the Tukey post hoc test was used. The level of significance was set at $p < 0.05$.

◂**Fig. 3** The knockout of SynII does not alter DSI in the DG. **a** Representative traces of eIPSCs from young WT (black trace) and young SynII KO (red trace) DG-GCs. **b** Bar graph of eEPSC amplitude recorded in WT (70.24 ± 14.45 pA) and SynII KO (121.80 ± 15.16 pA) mice ($n = 5$ neurons from 3 WT mice and n = 7 neurons from 4 SynII KO mice). *$p < 0.05$, two-tailed unpaired Student's t test ($t = 2.462$, df = 9.763). **c** Input/output curve curves obtained by plotting the amplitude of the eIPSCs as function of the stimulation intensity (from 50 to 250 µA) in WT and SynII KO mice. **d** Representative traces of the eIPSC-DSI. One eIPSC is reported as baseline representing 100% of the synaptic evoked response; after 5-s at 0 mV, three pulses were applied every 10-s. **e** eIPSC amplitude expressed in percent of baseline ($n = 7$ neurons from 3 WT mice and n = 7 neurons from 3 SynII KO mice). WT mice at $t_{1s} = 70.83 \pm 9.6\%$; SynII KO mice at $t_{1s} = 65.36 \pm 15.34\%$. *$p < 0.05$, one sample Student's t test ($t = 3.021$, df = 6 in WT and $t = 2.473$, df = 6 in SynII KO). The black and red asterisks represent the statistical significance for the WT and SynII KO groups, respectively. **f** Representative traces of eIPSCs from adult WT (black trace) and adult SynII KO (red trace) DG GCs. **g** Bar graph of eIPSC amplitude in WT (80.89 ± 9.20 pA) and SynII KO (132.60 ± 17.51 pA). *$p < 0.05$, two-tailed unpaired Student's t test ($t = 2.501$, df = 13). **h** Input/output curve curves obtained by plotting the amplitude of the eIPSCs as function of the stimulation intensity (from 50 to 250 µA) in 5–8 months WT and SynII KO mice ($n = 10$ neurons from 3 WT and $n = 9$ neurons from 3 SynII KO mice). WT mice at 200 µA = 110.6pA ± 7.6 pA and at 250 µA = 120.4 ± 9.4 pA; SynII KO mice at 200 µA = 186.5pA ± 31.86 pA and at 250 µA = 192.2 ± 27.6 pA. *$p < 0.05$, a two-tailed unpaired Student's t test ($t = 2.432$, df = 17 200µA and $t = 2.570$, df = 17 in 250µA). **i** Representative traces of the eIPSC-DSI experiment. One eIPSC is reported as baseline representing 100% of the synaptic response; after 5 s at 0 mV, three pulses were applied every 10 s. **j** eIPSC amplitude expressed in percent of baseline in WT and SynII KO mice

Results

The levels of the eCB and 2-AG, are altered in the hippocampus of SynII KO mice

The eCBs play a critical role in suppressing seizures in the hippocampus, and their levels are often altered in epilepsy [24]. To understand whether there is an alteration in the levels of the two major eCBs, 2-AG and AEA were quantified by LC-APCI-MS in young (1–2 months) and adult (5–8 months) SynII KO mice. We observed a strong decrease in 2-AG levels in the hippocampus of both groups of SynII KO mice compared with age-matched WT mice (Fig. 1a). Conversely, we found an age-dependent increase of AEA levels (Fig. 1b) irrespective of the genotype.

The hippocampal 2-AG levels are directly affected by the level of neuronal activity [32] and by the expression of the enzymes directly implicated in the 2-AG synthesis [33, 34], such as diacylglycerol lipase-α (DAGL-α [35]) or degradation, such as monoacylglycerol lipase (MAGL; [36]). We observed a reduction of DAGL-α in the dentate gyrus of both young and adult SynII KO mice (Fig. 2a–e), while no differences were observed in MAGL expression by matching the mice either by genotype or age (Fig. 2f). These data point to a reduced biosynthesis as a possible explanation for the reduction of 2-AG levels observed in SynII KO mice.

DSI is not altered in SynII KO mice

The DG contains a variety of inhibitory interneurons contacting the GCs [37]. In particular, cholecystokinin (CCK)-expressing basket cells are the primary CB1R-regulated source of inhibition of GCs. Expression of CB1Rs at their axon terminals distinguishes CCK interneurons from parvalbumin or somatostatin interneurons [38, 39].

We investigated whether the changes in eCB levels observed in the hippocampus of SynII KO mice have implications for the inhibitory input to GCs [27, 28]. We performed whole-cell voltage measurements of GCs in hippocampal slices of young and adult SynII KO mice and age-matched WT mice to analyse the DSI of eIPSCs and sIPSCs across genotype and age.

First, DSI was assessed by analysing the effect of GC depolarization on eIPSCs triggered by placing an extracellular electrode near the GC body in the DG molecular layer of young SynII KO [13, 40]. We observed an increase in eIPSC amplitude calculated using a minimal stimulation protocol, which confirms the previously shown upregulation of synchronous GABA release associated with SynII deletion [13] (Fig. 3a, b) or using input/output (I/O) protocol (Fig. 3c). DSI was assessed by recording baseline eIPSCs (holding voltage: − 80 mV). Subsequently, a 5-s depolarization step at 0 mV was applied, and the eIPSCs were recorded at intervals of 1, 10, and 21-s following the depolarizing step (Fig. 3d) [41]. DSI was present in both genotypes with no difference between the two groups (Fig. 3e).

No differences were found also when we analysed the basal frequency and amplitude of sIPSCs in either genotype (Supplementary Fig. 1a-c) and in the DSI calculated analysing the sIPSC frequency (Supplementary Fig. 1d, e), whereas the sIPSC amplitude showed only a mild decrease immediately after the end of the depolarizing step lasting only 5-s (Supplementary Fig. 1f). The involvement of the eCB system was confirmed in SynII KO mice using the CB1R antagonist AM251, which completely abolished the reduction in frequency and amplitude of sIPSCs observed after the depolarizing step (Supplementary Fig. 1 g, h).

As observed in young mice, we still detected an increment of eIPSC amplitude in adult SynII KO mice in comparison with aged-matched WT mice (Fig. 3f, g) at the minimal stimulation, that was maintained using an I/O protocol (Fig. 3h). However, unlike what previously observed in young mice, no DSI was detected in both adult WT and SynII KO mice based on eIPSC amplitude (Fig. 3i, j).

No differences were found in the basal frequency and amplitude of sIPSCs in old WT and SynII KO mice

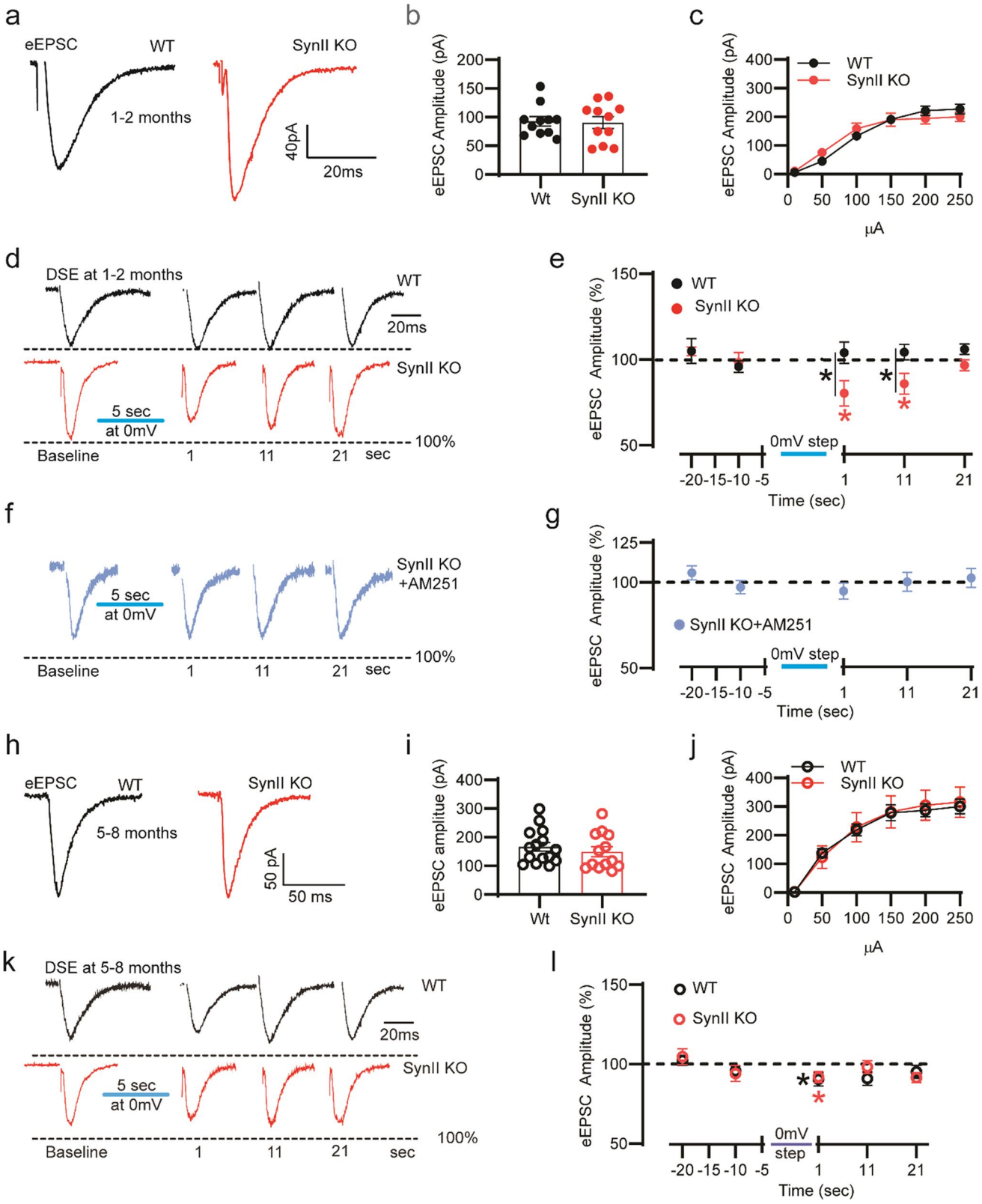

(Supplementary Fig. 2a–c). At the same time, the absence of DSI was confirmed analyzing the variation of the sIPSCs frequency respect to the baseline (Supplementary Fig. 2d, e).

These data are in line with other works showing that in patients with TLE, a reduction in CB1R expression is specifically observed in the excitatory fibres of the DG

◂**Fig. 4** DSE is enhanced in young Syn II KO mice. **a** Representative traces of eEPSCs from young WT (black trace) and aged-matched SynII KO (red trace) mouse in DG GCs. **b** Bar graph of eEPSC amplitude (WT = 92.84 ± 8.20 pA and SynII KO = 90.57 ± 10.38 pA). **c** Input/output curve curves obtained by plotting the amplitude of the eEPSCs as function of the stimulation intensity (from 50 to 250 µA) in 1–2 months WT and SynII KO mice ($n = 16$ neurons from 4 WT and $n = 13$ neurons from 3 SynII KO mice). WT mice at 50µA = 45pA ± 8.6pA; SynII KO mice at 50µA = 92.17pA ± 18.14pA. Two-tailed unpaired Student's t test ($t = 2.491$, df = 27, $^*p < 0.05$). **d** Representative traces of the eEPSC-DSE experiment. One eEPSC is reported as baseline representing 100% of the synaptic response; after 5 s at 0 mV, three pulses were applied every 10 s. **e** eEPSC amplitude expressed in percent of with respect to baseline ($n = 13$ neurons from 4 WT mice and $n = 11$ neurons from 4 SynII KO mice). WT mice $t_{1s} = 104 \pm 6.2$, $t_{11s} = 104.3 \pm 4.5\%$; SynII KO mice $t_{1s} = 80.41 \pm 7.3\%$, $t_{11s} = 85.93 \pm 6.10\%$. $^*p < 0.05$ (red asterisk for the SynII KO group), one sample Student's t test within genotype ($t = 2.659$, $df = 10$ in t_{1s} and $t = 2.299$, df = 10 in t_{11s},); $^*p < 0.05$ (black asterisk and line), two-tailed unpaired Student's t test across genotype ($t = 2.455$, df = 22 in t_{1s} and t = 2.458, df = 22 in t_{11s},). **f** Representative traces of the eEPSC-DSE experiment in SynII KO + AM251 slices. One eEPSC is reported as baseline representing 100% of the synaptic response; after 5-s at 0 mV, three pulses were applied every 10-s. **g** eEPSC amplitude expressed in percent of baseline in SynII KO mice in the presence of AM251. **h** Representative traces of eEPSCs from adult WT (black trace) and adult SynII KO (red trace) mouse in DG GCs. (**i**) Bar graph of eEPSC amplitude in adult WT (166.30 ± 15.48 pA) and adult Syn II KO (149.00 ± 17.64 pA). (**j**), (**c**) Input/output curve curves obtained by plotting the amplitude of the eEPSCs as function of the stimulation intensity (from 50 to 250 µA) in 5–8 months WT and SynII KO mice. **k** Representative traces of the DSE experiment in adult WT and SynII KO mice. One eEPSC is reported as baseline representing 100% of the synaptic response; after 5-s at 0 mV, other four pulses were applied every 10 s. **l** Percentage change of the eEPSC amplitude with respect to baseline ($n = 15$ neurons from 4 adult WT mice and $n = 13$ neurons from 4 adult SynII KO mice). WT mice at $t_{1s} = 90.51 \pm 4.30\%$, SynII KO mice at $t_{1s} = 91.95 \pm 3.50\%$. $^*p < 0.05$, one sample Student's t test ($t = 2.194$, df = 14 in WT mice and in $t = 2.286$, df = 12in SynII KO mice). The black and red asterisks represent the statistical significance for the WT and SynII KO groups, respectively

IML, in the absence of changes in CB1Rs in inhibitory axon terminals [42]. Moreover, the DG is particularly sensitive to ageing in both humans and rodents and a decline in the eCB system has been reported in middle-aged [43] and aged mice [44]. Overall, the analysis of DSI between young and adult WT and SynII KO showed disappearance of DSI in both genotypes, confirming the previously reported age-dependent decline of the eCBs modulation [43, 44] (Supplementary Fig. 2f).

The difference in DSE between WT and SynII KO mice disappears with age

It is well established that CB1Rs modulate excitatory inputs to the DG [45]. The primary source of excitation for the DG comes from the MCs [46] and the long-range projecting neurons of the entorhinal cortex passing through the molecular layer [7].

To analyse DSE in excitatory inputs to GCs in young and adult WT and SynII KO mice, an extracellular electrode was placed between the inner part of the molecular layer (IML) and the medial molecular layer (MML), which is reported to exhibit higher expression of CB1R [45, 47, 48]. Consistently with previous reports [13], no significant change in eEPSC amplitude was observed in young SynII KO mice compared with WT slices using a minimal stimulation protocol to activate the excitatory fibres contacting granule cells (Fig. 4a,b) or an I/O protocol (Fig. 4c). Conversely, a significant DSE was observed in slices from young SynII KO mice compared to age-matched WT controls, in which DSE was not observed (Fig. 4d, e). Such DSE, specific for young SynII KO mice, was totally abolished by AM251 (Fig. 4f, g), confirming the involvement of CB1Rs.

The comparison of eEPSC amplitude between adult symptomatic SynII KO and age-matched WT mice, recapitulated the absence of effects already observed in young mice using both protocol of stimulation (Fig. 4h–j). Interestingly, the eCB-dependent DSE, observed in young SynII KO mice but not in young WT mice, became similar between the two genotypes in adulthood (Fig. 4k, l).

Because the effect of the eCB-induced suppression of synaptic transmission was analysed in a 20-s time frame and since the sEPSC frequency in DG was ~ 20 times lower than that of sIPSCs in both young and adult WT and SynII KO mice, we limited our DSE analysis to the amplitude of eEPSCs (Supplementary Fig. 3). The data suggest that 2-AG/CB1R retrograde signalling plays a role in maintaining network stability in the pre-symptomatic period, delaying the appearance of the overt epileptic phenotype in SynII KO.

Excitatory synapses to granule cells are more responsive to the CB1R agonist ACEA

The increment of DSE in young SynII KO mice points to a possible tonic control of synaptic transmission; however, we did not observe genotypic differences when we recorded the amplitudes of eEPSCs (Fig. 5a) and eIPSCs (Fig. 5b) before and after the CB1R antagonist AM251. Since we observed a DSE in SynII KO, it is possible that the increased DSE might arise from increased CB1R sensitivity in those specific synapses, notwithstanding the lower levels of 2-AG. This possibility was assessed by testing ACEA, a synthetic endocannabinoid-like CB1R agonist, on the eEPSC amplitude. Indeed, we observed a significant reduction of eEPSC amplitude in 1–2 months SynII KO (~ 20%) with respect to WT (~ 7%) mice (Fig. 5c–e).

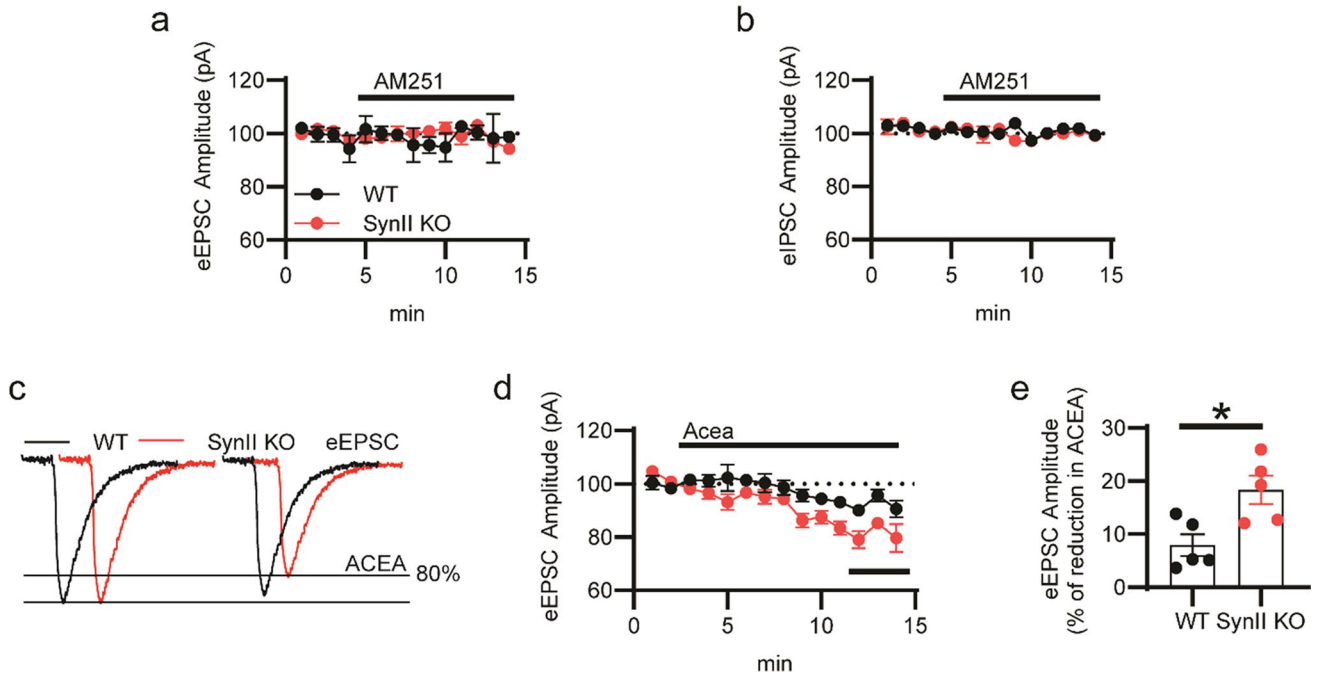

Fig. 5 CB1 sensitivity to agonists is increased in young SynII KO mice. **a** Percentage of eEPSC amplitude changes after addition of AM251 in comparison to the baseline in WT and SynII KO mice of 1–2 months of age. **b** Percentage of eIPSC amplitude changes after addition of AM251 in comparison to the baseline in WT and SynII KO mice of 1–2 months of age. **c** Representative scheme of eEPSC amplitude reduction in SynII KO mice (red traces) in the presence of the synthetic endocannabinoid-like CB1R agonist ACEA (125 nM). **d** Percentage of eEPSC amplitude changes after addition of ACEA in WT and SynII KO mice. **e** Bar graph of eEPSC amplitude reduction average calculated in the last 3 min of recording in WT + ACEA (7.9 ± 2%) and SynII KO + ACEA (18.36 ± 2.6%) mice (n = 5 neurons from 3 mice). *$p < 0.05$, two-tailed unpaired Student's t test ($t = 3.107$, df = 8)

CB1R expression changes in the DG parallel the changes in DSE/DSI expression in WT and SynII KO mice

Changes in DSI/DSE ratio depend on the expression pattern of CB1Rs. Since the marked decrease in hippocampal 2-AG levels observed in SynII KO mice cannot explain the stronger DSE observed in these animals and the disappearance of this effect with age, we sought to analyse CB1R expression in the DG in relation to the expression of VGLUT1 and VGAT, which label excitatory and inhibitory terminals, respectively. We observed significant increase in the extent of CB1R/VGLUT1 colocalization in the DG of SynII KO mice with respect to WT mice at 1–2 months of age that was lost at 5–8 months of age (Fig. 6a–c; Fig. 6m), consistent with the specific presence of DSE in young SynII KO mice and with its age-dependent decline. On the contrary, in both WT and SynII KO mice, the extent of CB1R/VGAT colocalization declined with age (Fig. 6g–l; Fig. 6n), consistent with the age-dependent decrease of DSI in both genotypes. Thus, both increased expression (present section) and increased agonist sensitivity (previous section) of CB1Rs likely explain the stronger DSE observed in young SynII KO mice.

CB1R antagonism increases seizure propensity in young SynII KO

Although an overt epileptic phenotype appears in SynII KO mice only after 2–3 months of age, it was reported that occasional seizures can be evoked in younger mice by suspending them by their tails [17]. Given the potential role of 2-AG/CB1R signalling in preserving network stability in the presymptomatic phase, we used this protocol in young SynII KO mice to check whether the blockade of CB1Rs increases seizure propensity. WT and SynII KO mice were tested in two sequential trials: mice were first treated with vehicle and, after 3 days, intraperitoneally injected with AM251. In WT mice, the administration of AM251 resulted in an increased percentage of the time of immobility and a parallel reduction of the time of movement, while SynII KO mice were fully insensitive to the treatment (Fig. 7a, b). Interestingly, CB1R antagonism in SynII KO mice resulted in a 20% increase in seizure duration (Fig. 7c) without affecting

the seizure latency (Fig. 7d). Conversely, the inhibition of MAGL with JZL184 induced a reduction of seizure duration with no changes in seizure latency (Fig. 7e, f).

Discussion

Epileptogenesis is a complex phenomenon involving a series of molecular, cellular, and network changes that occur over an extended period of time after the initial injury [49]. Studying the changes in synaptic transmission between the pre-epileptic and epileptic phases provides an opportunity to understand how a given neuronal network adapts to establish the correct E/I balance. The latent phase, which lasts months to years before the onset of the epileptic phenotype in humans, lasts from 2 to 12 weeks of life in SynII KO mice [50], an age at which the disruption of the correct E/I balance starts provoking seizures [21]. However, it is important to emphasize that evoked seizures can occur under certain stress conditions as early as 1–2 months of age [17].

An important matter of investigation is to understand the molecular and cellular mechanisms through which the full epileptic phenotype manifests late in postnatal development in these mice, although other phenotypic traits are altered much earlier [12]. SynII KO mice are characterized by a congenital deregulation of synaptic vesicle protein expression [51], which mainly affects GABA release [13, 15, 16]. The absence of *SYN2* leads to an increase in synchronous GABA release and a decrease in asynchronous GABA release [13, 15] at inhibitory synapses to GCs in the DG. This impairment has been directly linked to the loss of tonic inhibitory GABA currents, which may trigger the epileptic phenotype by increasing excitatory drive to GCs [14].

The eCBs, whose production is directly affected by the level of neuronal activity, are known to regulate the E/I balance and synchronize the activity between presynaptic and postsynaptic neurons by finely modulating synaptic strength through retrograde signalling. Indeed, the eCB system responds to the demands of homeostasis, which is an activity-dependent process [52]. Here, we show that retrograde eCB signalling at CB1Rs plays a role by tonically reducing the E/I ratio of DG-GCs in pre-symptomatic, but not symptomatic, SynII KO mice, and that CB1R antagonism accelerates the appearance of the overt epileptic phenotype in pre-symptomatic mice. It is interesting to note that CB1R antagonism in WT mice resulted in an increase in immobility duration, and a corresponding decrease in movement duration, which are consistent with previous data showing that silencing or pharmacological inhibition of CB1R [53] increases immobility in the TST, a proxy of a depressive state. This effect was not present in AM251-treated SynII KO mice, possibly because these animals spent a significant time having seizures. As reported for other epileptic models, the inhibition of MAGL with JZL184 caused the reduction of seizure duration in SynII KO during the TST [54, 55]. Although this behavioural paradigm is commonly used to test the antidepressant effect of drugs, it has also been used to induce seizures in the EL-mice, a model of temporal lobe epilepsy [56–58]. In addition, the recruitment of the hippocampal microcircuitry and DG during TST has been reported [59]. Schwark and coworkers showed that the reintroduction of SynII via AAV into the hippocampus and cortex of SynII KO mice reversed seizures triggered by TST [17]. On the other hand, another study showed that changes in hippocampal activity are causally related to TST-induced behaviour [60]. Thus, although the TST is not the paradigm of choice to test seizure susceptibility, it has been used in SynII KO mice to assess their vulnerability to seizures, demonstrating the existence of a causal relationship with hippocampal circuit recruitment in these mice.

Although the clarification of the molecular mechanism linking the knockout of SynII, a protein involved in the release of neurotransmitters, and neuron- and age-dependent changes in eCB signalling was not the scope of this study, we do provide evidence that the reduction in the concentrations of 2-AG might be due to the reduced expression of DAGL-α in the DG of SynII KO mice. The observed increase in CB1R expression and sensitivity to a synthetic agonist, observed in the ML of young SynII KO mice are likely the expression of a rearrangement of the DG network to counteract the congenital hyperexcitability [16]. Future work will be necessary to clarify this point (see further discussion on this issue below).

It is known that CB1Rs undergo long-lasting changes when neuronal activity is altered by epilepsy [61, 62] or by chronic application of CB1R agonists [63]. Evidence of how eCBs regulate synaptic plasticity in the hippocampal DG has been reported for inhibitory inputs from CCK interneurons [39] and excitatory inputs originating from MCs [64–66] and synapses of the medial and lateral perforant pathways (MPP and LPP) from the entorhinal cortex [67]. These three groups of GC-afferents form synapses in three different subregions of the molecular layer: the IML, the MML, and the outer molecular layer (OML) [7]. Chiu and Castillo reported that the short-term plasticity event of DSE regulates MC–GC, but not the MPP/LPP–GC, synapses [64], where eCBs appear to be mostly involved in regulating long-term plasticity [67]. In our DSE experiments, the extracellular electrode was placed near the GC at a location between the IML and the MML that, in principle, should anatomically exclude the LPP (Supplementary Fig. 4). Therefore, it is tempting to speculate that the increase in DSE specifically observed in pre-symptomatic SynII KO mice predominantly results from the excitatory input present in the IML synapses, where the MC-GC synapses are mainly located. Indeed, the increase in the E/I ratio caused by high-frequency stimulation of the

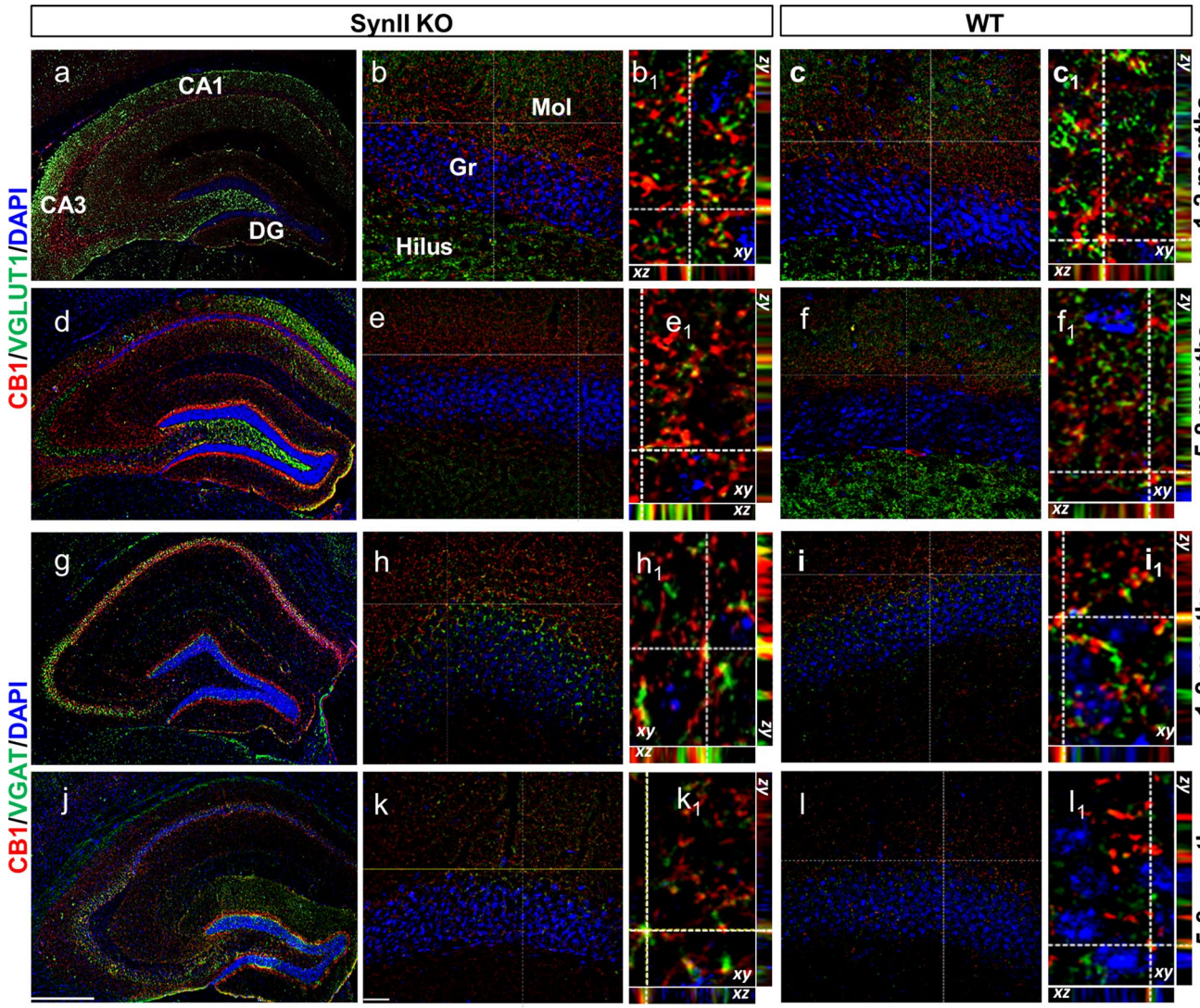
SynII KO
WT
CB1/VGLUT1/DAPI
CB1/VGAT/DAPI
1-2 months
5-8 months
CA1
CA3
DG
Mol
Gr
Hilus
xy
xz
zy

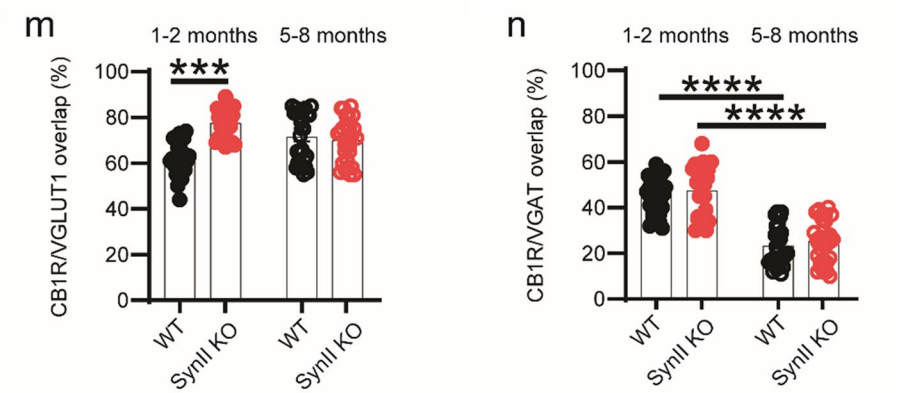
m
1-2 months
5-8 months
CB1R/VGLUT1 overlap (%)
***
WT
SynII KO
n
CB1R/VGAT overlap (%)
****

◂**Fig. 6** Distribution of CB1R immunoreactivity in glutamatergic and GABAergic inputs to the GCs in the DG of young and adult SynII KO mice. **a-f** CB1/VGLUT1/DAPI immunolabeling of the DG showing the increment of CB1/VGLUT1 colocalization in 1/2-month-old SynII KO in comparison to age-matched WT mice; this difference between the two genotypes is lost in 5/8-month-old mice. **g–l** CB1/VGAT/DAPI immunolabeling of the DG showing the reduction of CB1/VGAT colocalization in 5/8-month-old mice in comparison to age-matched mice of both genotypes. $\mathbf{b_1}$–$\mathbf{i_1}$ High-power fluorescent micrographs of orthogonal stacks are shown for each respective (**b**–**i**) areas; dotted lines and crosshairs are used to show 3D coordinates and define the area of interest. **m** Bar graph showing the percentage of overlap in the CB1R/VGLUT1 immunoreactivity areas in 1/2-month-old and 5/8-month-old mice. $n=30$ sections per group in three mice; $WT_{1/2}=62.13\pm1.30\%$, SynII $KO_{1/2}=77.43\pm1.10\%$, $WT_{5/8}=71.33\pm1.90\%$, SynII $KO_{5/8}=69.97\pm1.7\%$. $^{***}p<0.001$, two-way ANOVA ($F_{1,116}=19.65$)/Tukey's tests. **n** Bar graph showing the percentage of overlap in the CB1R/VGAT immunoreactivity areas in 1/2-month-old and 5/8-month-old mice. $n=30$ sections in three mice; $WT_{1/2}=45.07\pm1.4\%$, SynII $KO_{1/2}=47.47\pm1.90\%$, $WT_{5/8}=23.27\pm1.60\%$, SynII $KO_{5/8}=25.20\pm1.60\%$., $^{****}p<0.0001$, two-way ANOVA ($F_{1.116}=1.661$)/Tukey's tests

MC-GC synapses described by Toader and collaborators in both pre-symptomatic and epileptic SynII KO mice may be responsible for DG hyperexcitability [12]. In this view, eCBs could help balance this hyperexcitability in the first 2 months of life of SynII KO mice. Thus, it is possible that the enhanced DSE observed in pre-symptomatic SynII KO mice compensates for the decrease in tonic GABAergic inhibition and the increase in the excitatory drive of MC-GC synapses, at least in the first 2 months of life, thus delaying the appearance of epilepsy. The loss of DSE observed in 5–8-month-old SynII KO mice might be due to the large increase in BDNF detected in 6-month-old Syn II KO [22] and to the BDNF inhibition of CB1R function [68, 69].

A recent study examining eCB levels in brain samples from patients with TLE found that the concentration of 2-AG was reduced by 51% and 65% in the hippocampus and temporal cortex, respectively, whereas AEA did not change in the hippocampus [26]. These data are in line with

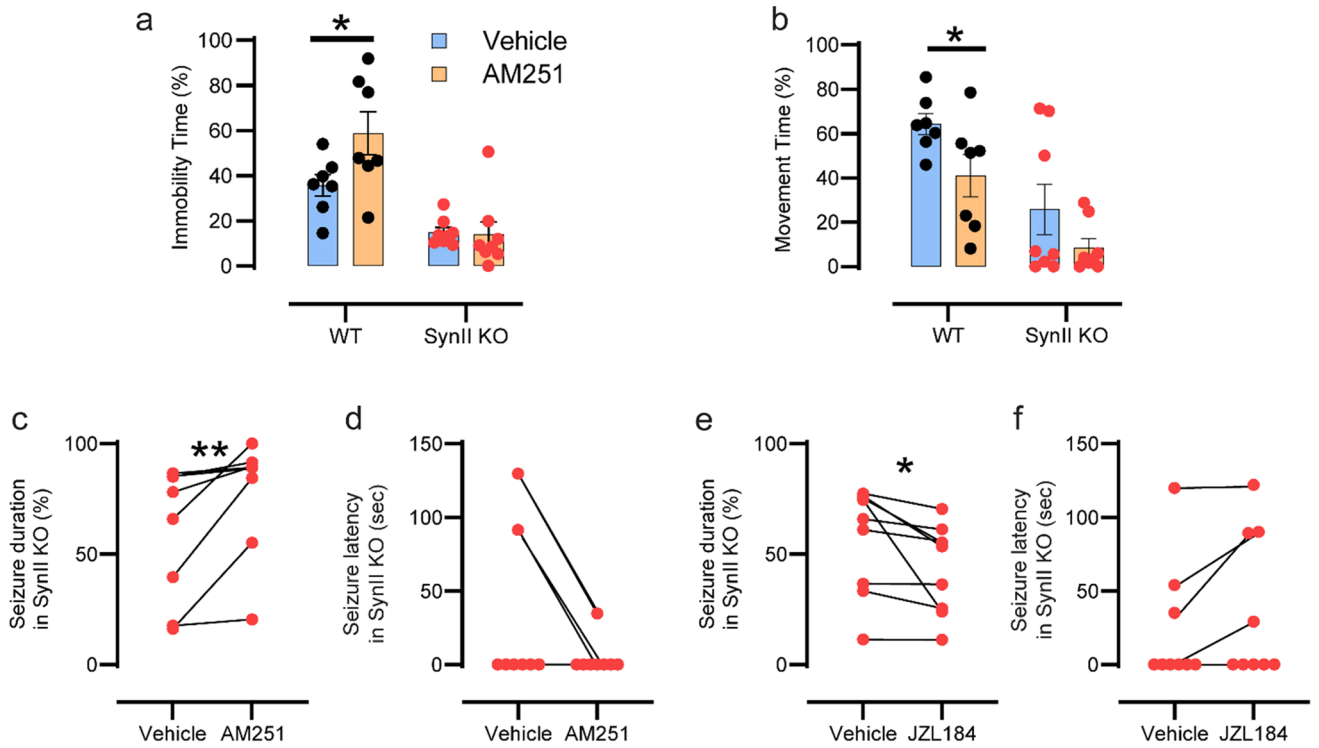

Fig. 7 Blockade of CB1Rs by AM251 increases seizure susceptibility in young SynII KO mice. **a** Percentage of immobility duration in the tail suspension test in 7 WT (vehicle = $35.66\pm12.64\%$, AM251 = $58.71\pm25.24\%$) and 8 SynII KO (vehicle = $14.91\pm5.90\%$, AM251 = $13.96\pm15.89\%$) mice before and after AM251 administration (3 mg/kg). $^{*}p<0.05$, two-way ANOVA ($F_{1,13}=5.427$)/Tukey's tests. **b** Percentage of movement duration in the tail suspension test in WT (vehicle = $64.34\%\pm4.7\%$, AM251 = $41.01\%\pm9.4\%$) and SynII KO (vehicle = $25.78\%\pm11.4\%$, AM251 = $8.6\%\pm4\%$) mice before and after AM251 administration. $^{*}p<0.05$, two-way ANOVA ($F_{1.13}=14.52$)/Tukey's tests. **c** Percentage of seizure duration in the tail suspension test in 8 SynII KO mice (vehicle = $59.31\pm30.39\%$, AM251 = $77.42\pm26.48\%$) before and after AM251 administration. $^{**}p<0.01$, Wilcoxon's matched-pairs signed rank test (sum of positive, negative ranks = 0.000, −36.00). **d** Seizure latency in SynII KO mice treated with vehicle and AM251. Note that the treatment reduced the latency time in three out of eight mice that displayed a latency > 0 s. **e** Percentage of seizure duration in the tail suspension test in 8 SynII KO mice (vehicle = $56.88\pm7.9\%$, JZL184 = $43.71\pm6.7\%$) before and after JZL184 administration. $^{**}p<0.01$, Wilcoxon's matched-pairs signed rank test (sum of positive, negative ranks = 45.00, 0.000). **f** Seizure latency in SynII KO mice treated with vehicle and JZL184. Note that the treatment induced non-significant changes in four out of nine mice

our LC–MS data showing a reduction of 2-AG in the hippocampus of SynII KO mice. While the lower levels of 2-AG in SynII KO mice may appear counterintuitive in view of their increased DSE, it is important to mention that these two pieces of data may not necessarily be interconnected. First, 2-AG levels were measured in the whole hippocampus, whereas DSE is an eCB-dependent effect specific of a particular hippocampal microcircuit LPP (Supplementary Fig. 4). Moreover, the distribution of CB1Rs at glutamatergic terminals controlling DSE in the DG is a more reliable proxy of eCB tone. In this respect, the significant increase of CB1R/VGLUT1 colocalization in young SynII KO and its attenuation with age closely parallels the precocious appearance of DSE in these mice and its age-dependent decline. Nevertheless, the observed age-independent reduction of 2-AG levels in SynII KO mice deserves attention for future studies aimed at investigating CB1R/CB2R-mediated neuromodulatory or anti-inflammatory effects in hippocampal areas other than the DG that might result impaired in this animal model of epilepsy.

Among the three major classes of inhibitory neurons in the DG, only CCK interneurons express CB1Rs. It remains unclear whether the age-dependent reduction in DSI and the CB1R/VGAT colocalization observed in both genotypes is due to a loss of CCK interneuron inputs to GC or to a reduction of CB1Rs in CCK interneuron terminals during aging. Previous studies have reported a decrease in CB1R density in the hippocampus during aging [70, 71]. At the network level, the loss of DSI at 5–8 months of age would theoretically lead to a reduction in the E/I ratio and to an increased circuit inhibition, whereas in SynII KO mice the inhibitory tone is severely altered resulting in mice becoming fully epileptic in the adulthood due to the concomitant loss of compensatory DSE at this age [13–16].

In summary, we have shown that: (1) the regulation of excitatory and inhibitory transmission to GCs by eCB signalling at CB1Rs evolves during the transition between presymptomatic and epileptic states in SynII KO mice, a murine genetic model of TLE; (2) the loss of this age-dependent eCB role in the maintenance of the E/I balance of GCs underlies seizure susceptibility in adult mice or young mice treated with a CB1R antagonist. Future studies will investigate the nature and exact location of other hippocampal eCB-mediated protective mechanisms that are defective in SynII KO mice and their relevance to clinical TLE.

Supplementary Information The online version contains supplementary material available at https://doi.org/10.1007/s00018-023-05029-7.

Acknowledgements The authors are grateful to Dr. Roberta Verde (ICB-CNR Pozzuoli, Italy) for technical support for LC–MS mass spectrometry.

Author contributions NF performed and analysed the electrophysiological experiments and statistical analysis, prepared the figures and wrote a drafted version of the manuscript; AN and AS performed behavioural experiments; BF, LA, and PG performed immunohistochemical experiments and data acquisition; FP performed LC–MS mass spectrometry analysis; AS performed behavioural experiments and analysis; PB and FB provided the SynII KO colony of mice and supervised electrophysiological study; PB, FB, VD, and LC supervised the study and wrote the final version of the manuscript. VD and LC conceptualized the study. All authors analysed and discussed the data, and edited and approved the final version of the manuscript.

Funding Financial support by the Joint International Research Unit (JIRU) for Chemical and Biomolecular Research on the Microbiome and its impact on Metabolic Health and Nutrition (MicroMeNu) and by the Sentinelle Nord Program of Université Laval (to N.F, L.C., and V.D.), which in turn is funded by the Canada First/Apogée program of the Tri-Agency of the Canadian Federal Government. Financial support by the Italian Ministry for University and Research (grant PRIN #2017M42834_002 to L.C. and 2017A9MK4R to F.B.) is also acknowledged.

Data availability The data and material that support the findings of this study are available upon request to the corresponding authors.

Declarations

Conflict of interest The authors have no relevant financial or non-financial interests to disclose.

Ethical approval All experiments were carried out in accordance with the guidelines established by the European Community Council (Directive 2010/63/EU of 22 September 2010) and were approved by the Italian Ministry of Health (n.26/2014, authorization n. 783/2020).

Consent to participate Not applicable.

Consent for publication Not applicable.

References

1. Beghi E, Giussani G, Nichols E et al (2019) Global, regional, and national burden of epilepsy, 1990–2016: a systematic analysis for the Global Burden of Disease Study 2016. Lancet Neurol 18:357–375. https://doi.org/10.1016/S1474-4422(18)30454-X
2. Fattorusso A, Matricardi S, Mencaroni E et al (2021) The pharmacoresistant epilepsy: an overview on existant and new emerging therapies. Front Neurol 12:674483. https://doi.org/10.3389/fneur.2021.674483
3. McIntosh WC, M Das J (2022) Temporal Seizure. In: StatPearls. StatPearls Publishing, Treasure Island (FL)
4. Boling W (2018) Surgical considerations of intractable mesial temporal lobe epilepsy. Brain Sci 8:35. https://doi.org/10.3390/brainsci8020035
5. Krook-Magnuson E, Armstrong C, Bui A et al (2015) *In vivo* evaluation of the dentate gate theory in epilepsy: Dentate gate in temporal lobe epilepsy. J Physiol 593:2379–2388. https://doi.org/10.1113/JP270056
6. Scharfman HE (2019) The dentate gyrus and temporal lobe epilepsy: an "exciting" era. Epilepsy Curr 19:249–255. https://doi.org/10.1177/1535759719855952

7. Amaral DG, Scharfman HE, Lavenex P (2007) The dentate gyrus: fundamental neuroanatomical organization (dentate gyrus for dummies). In: Progress in Brain Research. Elsevier, pp 3–790
8. Hsu D (2007) The dentate gyrus as a filter or gate: a look back and a look ahead. In: Progress in Brain Research. Elsevier, pp 601–613
9. London M, Häusser M (2005) Dendritic computation. Annu Rev Neurosci 28:503–532. https://doi.org/10.1146/annurev.neuro.28.061604.135703
10. Vyleta NP, Borges-Merjane C, Jonas P (2016) Plasticity-dependent, full detonation at hippocampal mossy fiber–CA3 pyramidal neuron synapses. Elife 5:e17977. https://doi.org/10.7554/eLife.17977
11. Henze DA, Wittner L, Buzsáki G (2002) Single granule cells reliably discharge targets in the hippocampal CA3 network in vivo. Nat Neurosci 5:790–795. https://doi.org/10.1038/nn887
12. Toader O, Forte N, Orlando M et al (2013) Dentate gyrus network dysfunctions precede the symptomatic phase in a genetic mouse model of seizures. Front Cell Neurosci. https://doi.org/10.3389/fncel.2013.00138
13. Medrihan L, Cesca F, Raimondi A et al (2013) Synapsin II desynchronizes neurotransmitter release at inhibitory synapses by interacting with presynaptic calcium channels. Nat Commun 4:1512. https://doi.org/10.1038/ncomms2515
14. Medrihan L, Ferrea E, Greco B et al (2015) Asynchronous GABA release is a key determinant of tonic inhibition and controls neuronal excitability: a study in the synapsin II $^{-/-}$ Mouse. Cereb Cortex 25:3356–3368. https://doi.org/10.1093/cercor/bhu141
15. Feliciano P, Matos H, Andrade R, Bykhovskaia M (2017) Synapsin II regulation of gabaergic synaptic transmission is dependent on interneuron subtype. J Neurosci 37:1757–1771. https://doi.org/10.1523/JNEUROSCI.0844-16.2016
16. Feliciano P, Andrade R, Bykhovskaia M (2013) Synapsin II and Rab3a cooperate in the regulation of epileptic and synaptic activity in the CA1 region of the hippocampus. J Neurosci 33:18319–18330. https://doi.org/10.1523/JNEUROSCI.5293-12.2013
17. Schwark R, Andrade R, Bykhovskaia M (2022) Synapsin II directly suppresses epileptic seizures in vivo. Brain Sci 12:325. https://doi.org/10.3390/brainsci12030325
18. Cavalleri GL, Weale ME, Shianna KV et al (2007) Multicentre search for genetic susceptibility loci in sporadic epilepsy syndrome and seizure types: a case-control study. Lancet Neurol 6:970–980. https://doi.org/10.1016/S1474-4422(07)70247-8
19. Lakhan R, Kalita J, Misra UK et al (2010) Association of intronic polymorphism rs3773364 A>G in synapsin-2 gene with idiopathic epilepsy. Synap N Y N 64:403–408. https://doi.org/10.1002/syn.20740
20. Prasad DKV, Shaheen U, Satyanarayana U et al (2014) Association of GABRA6 1519 T>C (rs3219151) and Synapsin II (rs37733634) gene polymorphisms with the development of idiopathic generalized epilepsy. Epilepsy Res 108:1267–1273. https://doi.org/10.1016/j.eplepsyres.2014.07.001
21. Etholm L, Bahonjic E, Walaas SI et al (2012) Neuroethologically delineated differences in the seizure behavior of Synapsin 1 and Synapsin 2 knock-out mice. Epilepsy Res 99:252–259. https://doi.org/10.1016/j.eplepsyres.2011.12.004
22. Barbieri R, Contestabile A, Ciardo MG et al (2018) Synapsin I and Synapsin II regulate neurogenesis in the dentate gyrus of adult mice. Oncotarget 9:18760–18774. https://doi.org/10.18632/oncotarget.24655
23. Chugh D, Ali I, Bakochi A et al (2015) Alterations in brain inflammation, synaptic proteins, and adult hippocampal neurogenesis during epileptogenesis in mice lacking synapsin2. PLoS ONE 10:e0132366. https://doi.org/10.1371/journal.pone.0132366
24. Sugaya Y, Kano M (2021) Endocannabinoid-mediated control of neural circuit excitability and epileptic seizures. Front Neural Circuits 15:781113. https://doi.org/10.3389/fncir.2021.781113
25. Kano M, Ohno-Shosaku T, Hashimotodani Y et al (2009) Endocannabinoid-mediated control of synaptic transmission. Physiol Rev 89:309–380. https://doi.org/10.1152/physrev.00019.2008
26. Rocha L, Cinar R, Guevara-Guzmán R et al (2020) Endocannabinoid system and cannabinoid 1 receptors in patients with pharmacoresistant temporal lobe epilepsy and comorbid mood disorders. Front Behav Neurosci 14:52. https://doi.org/10.3389/fnbeh.2020.00052
27. Kreitzer AC, Regehr WG (2001) Retrograde inhibition of presynaptic calcium influx by endogenous cannabinoids at excitatory synapses onto purkinje cells. Neuron 29:717–727. https://doi.org/10.1016/S0896-6273(01)00246-X
28. Isokawa M, Alger BE (2005) Retrograde endocannabinoid regulation of GABAergic inhibition in the rat dentate gyrus granule cell: Endogenous cannabinoid transmission in the dentate gyrus. J Physiol 567:1001–1010. https://doi.org/10.1113/jphysiol.2005.094219
29. Liu YB, Ye G-L, Liu X-S et al (1998) GABA $_A$ currents in immature dentate gyrus granule cells. J Neurophysiol 80:2255–2267. https://doi.org/10.1152/jn.1998.80.5.2255
30. Bolte S, Cordelières FP (2006) A guided tour into subcellular colocalization analysis in light microscopy. J Microsc 224:213–232. https://doi.org/10.1111/j.1365-2818.2006.01706.x
31. Can A, Dao DT, Terrillion CE et al (2011) The tail suspension test. J Vis Exp. https://doi.org/10.3791/3769
32. Cristino L, Bisogno T, Di Marzo V (2020) Cannabinoids and the expanded endocannabinoid system in neurological disorders. Nat Rev Neurol 16:9–29. https://doi.org/10.1038/s41582-019-0284-z
33. Massa F, Mancini G, Schmidt H et al (2010) Alterations in the hippocampal endocannabinoid system in diet-induced obese mice. J Neurosci 30:6273–6281. https://doi.org/10.1523/JNEUROSCI.2648-09.2010
34. Hashimotodani Y, Ohno-Shosaku T, Kano M (2007) Presynaptic monoacylglycerol lipase activity determines basal endocannabinoid tone and terminates retrograde endocannabinoid signaling in the hippocampus. J Neurosci Off J Soc Neurosci 27:1211–1219. https://doi.org/10.1523/JNEUROSCI.4159-06.2007
35. Reisenberg M, Singh PK, Williams G, Doherty P (2012) The diacylglycerol lipases: structure, regulation and roles in and beyond endocannabinoid signalling. Philos Trans R Soc B Biol Sci 367:3264–3275. https://doi.org/10.1098/rstb.2011.0387
36. Scalvini L, Piomelli D, Mor M (2016) Monoglyceride lipase: Structure and inhibitors. Chem Phys Lipids 197:13–24. https://doi.org/10.1016/j.chemphyslip.2015.07.011
37. Houser CR (2007) Interneurons of the dentate gyrus: an overview of cell types, terminal fields and neurochemical identity. In: Progress in Brain Research. Elsevier, pp 217–811
38. Katona I, Sperlágh B, Sík A, et al (1999) Presynaptically located CB1 cannabinoid receptors regulate GABA release from axon terminals of specific hippocampal interneurons. J Neurosci 19:4544–4558. https://doi.org/10.1523/JNEUROSCI.19-11-04544.1999
39. Hefft S, Jonas P (2005) Asynchronous GABA release generates long-lasting inhibition at a hippocampal interneuron–principal neuron synapse. Nat Neurosci 8:1319–1328. https://doi.org/10.1038/nn1542
40. Forte N, Binda F, Contestabile A et al (2020) Synapsin I synchronizes GABA release in distinct interneuron subpopulations. Cereb Cortex 30:1393–1406. https://doi.org/10.1093/cercor/bhz174
41. Wilson RI, Nicoll RA (2001) Endogenous cannabinoids mediate retrograde signalling at hippocampal synapses. Nature 410:588–592. https://doi.org/10.1038/35069076
42. Ludányi A, Erőss L, Czirják S et al (2008) Downregulation of the CB $_1$ cannabinoid receptor and related molecular elements

of the endocannabinoid system in epileptic human hippocampus. J Neurosci 28:2976–2990. https://doi.org/10.1523/JNEUROSCI.4465-07.2008
43. Amani M, Lauterborn JC, Le AA et al (2021) Rapid aging in the perforant path projections to the rodent dentate gyrus. J Neurosci 41:2301–2312. https://doi.org/10.1523/JNEUROSCI.2376-20.2021
44. Piyanova A, Lomazzo E, Bindila L et al (2015) Age-related changes in the endocannabinoid system in the mouse hippocampus. Mech Ageing Dev 150:55–64. https://doi.org/10.1016/j.mad.2015.08.005
45. Kawamura Y, Fukaya M, Maejima T et al (2006) The CB1 cannabinoid receptor is the major cannabinoid receptor at excitatory presynaptic sites in the hippocampus and cerebellum. J Neurosci 26:2991–3001. https://doi.org/10.1523/JNEUROSCI.4872-05.2006
46. Scharfman HE (1995) Electrophysiological evidence that dentate hilar mossy cells are excitatory and innervate both granule cells and interneurons. J Neurophysiol 74:179–194. https://doi.org/10.1152/jn.1995.74.1.179
47. Katona I, Urbán GM, Wallace M et al (2006) Molecular composition of the endocannabinoid system at glutamatergic synapses. J Neurosci 26:5628–5637. https://doi.org/10.1523/JNEUROSCI.0309-06.2006
48. Forte N, Boccella S, Tunisi L et al (2021) Orexin-A and endocannabinoids are involved in obesity-associated alteration of hippocampal neurogenesis, plasticity, and episodic memory in mice. Nat Commun 12:6137–6137. https://doi.org/10.1038/s41467-021-26388-4
49. Lignani G, Baldelli P, Marra V (2020) Homeostatic plasticity in epilepsy. Front Cell Neurosci 14:197. https://doi.org/10.3389/fncel.2020.00197
50. Rakhade SN, Jensen FE (2009) Epileptogenesis in the immature brain: emerging mechanisms. Nat Rev Neurol 5:380–391. https://doi.org/10.1038/nrneurol.2009.80
51. Rosahl TW, Spillane D, Missler M et al (1995) Essential functions of synapsins I and II in synaptic vesicle regulation. Nature 375:488–493. https://doi.org/10.1038/375488a0
52. Kim J, Alger BE (2010) Reduction in endocannabinoid tone is a homeostatic mechanism for specific inhibitory synapses. Nat Neurosci 13:592–600. https://doi.org/10.1038/nn.2517
53. Soriano D, Brusco A, Caltana L (2021) Further evidence of anxiety- and depression-like behavior for total genetic ablation of cannabinoid receptor type 1. Behav Brain Res 400:113007. https://doi.org/10.1016/j.bbr.2020.113007
54. Von Rüden EL, Bogdanovic RM, Wotjak CT, Potschka H (2015) Inhibition of monoacylglycerol lipase mediates a cannabinoid 1-receptor dependent delay of kindling progression in mice. Neurobiol Dis 77:238–245. https://doi.org/10.1016/j.nbd.2015.03.016
55. Sugaya Y, Yamazaki M, Uchigashima M et al (2016) Crucial roles of the endocannabinoid 2-arachidonoylglycerol in the suppression of epileptic seizures. Cell Rep 16:1405–1415. https://doi.org/10.1016/j.celrep.2016.06.083
56. Todorova MT, Burwell TJ, Seyfried TN (1999) Environmental risk factors for multifactorial epilepsy in EL Mice. Epilepsia 40:1697–1707. https://doi.org/10.1111/j.1528-1157.1999.tb01586.x
57. Leussis MP, Heinrichs SC (2006) Routine tail suspension husbandry facilitates onset of seizure susceptibility in EL mice. Epilepsia 47:801–804. https://doi.org/10.1111/j.1528-1167.2006.00525.x
58. Lee T-S, Li AY, Rapuano A et al (2021) Gene expression in the epileptic (EL) mouse hippocampus. Neurobiol Dis 147:105152. https://doi.org/10.1016/j.nbd.2020.105152
59. Hiraoka K, Motomura K, Yanagida S et al (2017) Pattern of c-Fos expression induced by tail suspension test in the mouse brain. Heliyon 3:e00316. https://doi.org/10.1016/j.heliyon.2017.e00316
60. Mineur YS, Obayemi A, Wigestrand MB et al (2013) Cholinergic signaling in the hippocampus regulates social stress resilience and anxiety- and depression-like behavior. Proc Natl Acad Sci 110:3573–3578. https://doi.org/10.1073/pnas.1219731110
61. Chen K, Ratzliff A, Hilgenberg L et al (2003) Long-term plasticity of endocannabinoid signaling induced by developmental febrile seizures. Neuron 39:599–611. https://doi.org/10.1016/S0896-6273(03)00499-9
62. Ye M, Monroe SK, Gay SM et al (2022) Coordinated regulation of CB1 cannabinoid receptors and anandamide metabolism stabilizes network activity during homeostatic downscaling. eNeuro 9:ENEURO.0276-22.2022. https://doi.org/10.1523/ENEURO.0276-22.2022
63. Augustin SM, Lovinger DM (2022) Synaptic changes induced by cannabinoid drugs and cannabis use disorder. Neurobiol Dis 167:105670. https://doi.org/10.1016/j.nbd.2022.105670
64. Chiu CQ, Castillo PE (2008) Input-specific plasticity at excitatory synapses mediated by endocannabinoids in the dentate gyrus. Neuropharmacology 54:68–78. https://doi.org/10.1016/j.neuropharm.2007.06.026
65. Uchigashima M, Yamazaki M, Yamasaki M et al (2011) Molecular and morphological configuration for 2-arachidonoylglycerol-mediated retrograde signaling at mossy cell-granule cell synapses in the dentate gyrus. J Neurosci 31:7700–7714. https://doi.org/10.1523/JNEUROSCI.5665-10.2011
66. Jensen KR, Berthoux C, Nasrallah K, Castillo PE (2021) Multiple cannabinoid signaling cascades powerfully suppress recurrent excitation in the hippocampus. Proc Natl Acad Sci 118:e2017590118. https://doi.org/10.1073/pnas.2017590118
67. Wang W, Trieu BH, Palmer LC et al (2016) A primary cortical input to hippocampus expresses a pathway-specific and endocannabinoid-dependent form of long-term potentiation. Eneuro 3:ENEURO.0160-16.2016. https://doi.org/10.1523/ENEURO.0160-16.2016
68. De Chiara V, Angelucci F, Rossi S et al (2010) Brain-derived neurotrophic factor controls cannabinoid CB1 receptor function in the striatum. J Neurosci 30:8127–8137. https://doi.org/10.1523/JNEUROSCI.1683-10.2010
69. Ferreira FF, Ribeiro FF, Rodrigues RS et al (2018) Brain-derived neurotrophic factor (BDNF) role in cannabinoid-mediated neurogenesis. Front Cell Neurosci 12:441. https://doi.org/10.3389/fncel.2018.00441
70. Canas PM, Duarte JMN, Rodrigues RJ et al (2009) Modification upon aging of the density of presynaptic modulation systems in the hippocampus. Neurobiol Aging 30:1877–1884. https://doi.org/10.1016/j.neurobiolaging.2008.01.003
71. Berrendero F, Romero J, Garcia-Gil L et al (1998) Changes in cannabinoid receptor binding and mRNA levels in several brain regions of aged rats. Biochim Biophys Acta BBA-Mol Basis Dis 1407:205–214. https://doi.org/10.1016/S0925-4439(98)00042-8